

**Structure and evolutionary trace-assisted screening of a residue swapping the substrate ambiguity and chiral specificity in an esterase**

Cea-Rama, Isabel; Coscolín, Cristina; Katsonis, Pangiotis; Bargiela, Rafael; Golyshin, Peter; Lichtarge, Olivier; Ferrer, Manuel; Sanz-Aparicio, Julia

Computational and Structural Biotechnology Journal

DOI:

[10.1016/j.csbj.2021.04.041](https://doi.org/10.1016/j.csbj.2021.04.041)

E-pub ahead of print: 18/04/2021

Peer reviewed version

[Cyswllt i'r cyhoeddiad / Link to publication](#)

Dyfyniad o'r fersiwn a gyhoeddwyd / Citation for published version (APA):

Cea-Rama, I., Coscolín, C., Katsonis, P., Bargiela, R., Golyshin, P., Lichtarge, O., Ferrer, M., & Sanz-Aparicio, J. (2021). Structure and evolutionary trace-assisted screening of a residue swapping the substrate ambiguity and chiral specificity in an esterase. *Computational and Structural Biotechnology Journal*, 19, 2307-2317. <https://doi.org/10.1016/j.csbj.2021.04.041>

Hawliau Cyffredinol / General rights

Copyright and moral rights for the publications made accessible in the public portal are retained by the authors and/or other copyright owners and it is a condition of accessing publications that users recognise and abide by the legal requirements associated with these rights.

- Users may download and print one copy of any publication from the public portal for the purpose of private study or research.
- You may not further distribute the material or use it for any profit-making activity or commercial gain
- You may freely distribute the URL identifying the publication in the public portal ?

Take down policy

If you believe that this document breaches copyright please contact us providing details, and we will remove access to the work immediately and investigate your claim.

Structure and evolutionary trace-assisted screening of a residue swapping the substrate ambiguity and chiral specificity in an esterase

Isabel Cea-Rama^{a, 1}, Cristina Coscolín^{b, 1}, Panagiotis Katsonis^c, Rafael Bargiela^d, Peter N. Golyshin^{d,e}, Olivier Lichtarge^c, Manuel Ferrer^{b,*}, and Julia Sanz-Aparicio^{a,*}

^a*Institute of Physical Chemistry "Rocasolano", CSIC, 28006 Madrid, Spain*

^b*Institute of Catalysis, CSIC, 28049 Madrid, Spain*

^c*Baylor College of Medicine, Houston, TX 77030, USA*

^d*Centre for Environmental Biotechnology, Bangor University, LL57 2UW Bangor, UK*

^e*School of Natural Sciences, Bangor University, LL57 2UW Bangor, UK*

¹These authors contributed equally to this work.

*Corresponding authors at: Institute of Physical Chemistry "Rocasolano", CSIC, Serrano 119, 28006 Madrid, Spain (J. Sanz-Aparicio). Institute of Catalysis, CSIC, Marie Curie 2, 28049 Madrid, Spain (M. Ferrer).

E-mail addresses: xjulia@iqfr.csic.es (J. Sanz-Aparicio), mferrer@icp.csic.es (M. Ferrer)

Phone numbers: +34915619400 (J. Sanz-Aparicio), +34915854872 (M. Ferrer)

Abbreviations: E_{app} , apparent enantioselectivity; ET, evolutionary trace; EA, evolutionary action; HEPES, 40 mM 4-(2-hydroxyethyl)-1-piperazineethanesulfonic acid; Ni-NTA, nickel-nitrilotriacetic acid.

Short title: Tracing position swapping specificity

1 ABSTRACT

2
3 Our understanding of enzymes with high substrate ambiguity remains limited because their
4 large active sites allow substrate docking freedom to an extent that seems incompatible with
5 stereospecificity. One possibility is that some of these enzymes evolved a set of
6 evolutionarily fitted sequence positions that stringently allow switching substrate ambiguity
7 and chiral specificity. To explore this hypothesis, we targeted for mutation a serine ester
8 hydrolase (EH₃) that exhibits an impressive 71-substrate repertoire but is not stereospecific
9 (*e.e.* 50%). We used structural actions and a computational approach, the evolutionary trace
10 method, to explore specificity-swapping sequence positions and hypothesized that position
11 I244 was critical. Driven by evolutionary action analysis, this position was substituted to
12 leucine, which together with isoleucine appears to be the amino acid most commonly
13 present in the closest homologous sequences (max. identity, *ca.* 67.1%), and to
14 phenylalanine, which appears in distant homologues. While the I244L mutation did not have
15 any functional consequences, the I244F mutation allowed the esterase to maintain a
16 remarkable 53-substrate range while gaining stereospecificity properties (*e.e.* 99.99%).
17 These data support the possibility that some enzymes evolve sequence positions that
18 control the substrate scope and stereospecificity. Such residues, which can be evolutionarily
19 screened, may serve as starting points for further designing substrate-ambiguous but chiral-
20 specific enzymes that are greatly appreciated in biotechnology and synthetic chemistry.

21
22 Keywords: crystal structure; esterase; evolutionary trace; promiscuity; protein engineering;
23 specificity.

24 25 1. Introduction

26
27 The pivotal assets provided by the use of enzymes in industrial processes and consumer
28 products include the following: a lower energy footprint; reduced waste production and
29 chemical consumption; safer process conditions; and the use of renewable feedstocks. As
30 such, replacing chemicals (including chemical catalysts) with enzymes in industrial processes
31 or consumer products is expected to positively impact greenhouse gas emissions (reported
32 savings from 0.3 to 990 kg CO₂ equivalent/kg product) and global warming issues by
33 reducing water and energy consumption (estimates: 6000 million m³ and 167 TWh,
34 respectively) [1]. In particular, enzymes with broad substrate ambiguity and exact stereo-
35 control are appreciated as candidates for developing alternative methods to conventional
36 chemical catalysis in bench work and the pharmaceutical industry [2,3]. However, enzymes
37 that combine both features are rare. Indeed, most enzymes designed by nature through four
38 billion years of evolution perform primary reactions with exquisite specificity [4]. The
39 universe of enzymes with ambiguous specificities is also large, but the voluminous active
40 sites selected in evolution to provide a high level of substrate docking freedom are
41 commonly not stereospecific [5], which limits the technological potential of multi-specific (or
42 substrate-ambiguous) enzymes. A better understanding of how substrate specificity can be
43 modulated in such enzymes would assist engineering strategies [6] in increasing their
44 technological impact.

45 Past studies have shown that enzyme specificity is influenced by the architecture (size
46 and geometry) of their active-site cavity and by their access tunnels [7], which can evolve
47 from an ancestral core domain or a minimal structural unit within a superfamily [8]. In

48 general, large active sites are consistent with the very broad substrate specificity of these
49 enzymes, whereas enzymes with smaller and occluded cavities cannot readily accommodate
50 a larger number of substrates [7,9]. Aside from these general trends, the presence of key
51 substitutions in the active site and in the access tunnels [10,11] or the positioning of water
52 molecules [12] or anions [13] in the proximity of the active site may influence the entrance
53 and positioning of certain substrates. In other cases, alterations in specificity were ascribed
54 to large structural elements that are inserted, removed or rearranged in the sequence [14]
55 or to differences in the protein dynamics [15]. Few substitutions were also found to be
56 sufficient to modify the reaction mechanisms of enzymes, which opens the possibility to
57 transform distinct molecules [16]. These studies exemplify that influencing and expanding
58 the substrate specificity of enzymes is feasible. Prominent examples with remarkable
59 substrate specificity are the human cytochrome P450 enzyme [17] and resurrected TEM-1 β -
60 lactamases [18]. The application of multiple engineering methodologies has also
61 demonstrated that the transformation of a nonspecific enzyme into a specific enzyme is also
62 theoretically feasible [11,19-22], with this transformation being more effective when altering
63 residues close to the active site or the substrate accessibility channel [23,24].

64 While modulating substrate specificity in enzymes is thus feasible when examined as
65 separate properties, introducing chiral specificity to an enzyme with prominent substrate
66 ambiguity is challenging and has received much less attention. Few examples have been
67 reported, such as engineered horseradish peroxidase [25], cytochrome CYP3A4 [26],
68 peroxidase C45 [27], Michaelase [28], beta-lactamases [29] or esterase [30], which showed
69 chiral specificity while having moderate substrate ambiguity; however, in most cases,
70 specificity was established on the basis of a limited set of structurally similar substrates.

71 Here, we exploit previous comprehensive information on the substrate specificity of a
72 large set of ester hydrolases [9] tested with close to one hundred distinct esters to identify
73 one such enzyme, EH₃, which has remarkable multi-specificity, with sequence positions that
74 modulate both substrate ambiguity and chiral specificity. We focused on carboxylic ester
75 hydrolases (EC 3.1.1), as they are among the most important biocatalysts in the field of
76 biotechnology [31], and because of their capacity to catalyze hydrolysis with exquisite
77 enantio-, regio-, and stereospecificity. According to their sequence, they are grouped into 19
78 different families with more than 1,500 available protein structures according to the lipase
79 engineering database [32]. Through this investigation, we asked the following questions: Are
80 there sequence positions that determine enzyme specificity? Can these positions be
81 screened and used to produce substrate-promiscuous but chiral-specific enzymes?
82 Answering these questions may be fundamental from a basic point of view. Thus, functional
83 residues in enzymes tend to be highly conserved over evolution [33,34], but to what extent
84 certain sites impose substrate ambiguity over chiral specificity and, conversely, their
85 conservation through evolution are not known. This is of special significance given that
86 genome-scale model simulations and laboratory evolution experiments have shown that few
87 mutations shift enzyme substrate turnover rates toward new substrates, thus shaping
88 microbial adaptation to novel growth substrates [35]. From a technological point of view,
89 answering these questions will also have implications for fine-tuning enzyme specificity. For
90 the purpose of this study, we herein explore the evolutionary importance of sequence
91 positions that possibly have functional roles in the chiral specificity of substrate ambiguous
92 esterase through the application of a software program called Evolutionary Trace [36,37]
93 and structure-assisted and experimental validations. We would like to highlight that previous
94 work on evolutionary traces [38] focused on altering the substrate specificity for a few

95 substrates, and to the best of our knowledge, their application to modulate enzyme
96 specificity in combination with substrate promiscuity has not yet been reported.

97

98 **2. Materials and methods**

99

100 *2.1. Enzyme source, production and purification*

101 The vector pBXNH3 and the host *Escherichia coli* MC1061 were the sources of His₆-tagged
102 EH₃ (GenBank acc. nr. KY483645), a serine ester hydrolase isolated from the metagenomic
103 DNA of microbial communities inhabiting the chronically polluted seashore area of Milazzo
104 Harbor in Sicily [9]. The soluble His-tagged protein was produced and purified at 4°C after
105 binding to a Ni-NTA His-Bind resin (from Merck Life Science S.L.U., Madrid, Spain) as
106 described previously [39]. The purity was assessed as >98% using SDS-PAGE analysis in a
107 Mini PROTEAN electrophoresis system (Bio-Rad, Madrid, Spain). Purified protein was stored
108 at -86°C until use at a concentration of 10 mg ml⁻¹ in 40 mM 4-(2-hydroxyethyl)-1-
109 piperazineethanesulfonic acid (HEPES) buffer (pH 7.0). A total of approximately 20 mg of
110 total purified recombinant protein was obtained from a 1-liter culture.

111

112 *2.2. Source of chemicals*

113 The source or brand for each of the esters [purity ≥99%] used in this study has been
114 described previously [9]. Methyl-(*R*)-2-phenylpropanoate and methyl-(*S*)-2-
115 phenylpropanoate [purity ≥99%] were purchased from Combi-Blocks (San Diego, CA, USA).
116 HEPES [purity ≥99%] was purchased from Fisher Bioreagent (Ottawa, ON, USA). All other
117 chemicals [with the highest purity available] were purchased from Merck Life Science S.L.U.,
118 Madrid, Spain) and Sigma-Aldrich Química S.A. Madrid (Spain).

119

120 *2.3. Crystallization and X-ray structure determination of EH₃ complexed with methyl-(*R/S*)-2-phenylpropanoate*

122 The crystallization conditions reported for the native protein were optimized by
123 adjusting the protein and precipitant concentrations. The best crystals were grown by using
124 1 μl of EH_{3S192A} (20-60 mg ml⁻¹ in 40 mM HEPES (pH 7) and 100 mM NaCl) and 0.5 μl of
125 precipitant solution (28-29% PEG3000, 0.1 M Bis-tris (pH 6.5), and 0.2 M MgCl₂·6H₂O). The
126 complexes were obtained by soaking thin plate-shaped crystals of EH_{3S192A} in mother liquor
127 supplemented with 10-20 mM methyl-(*S/R*)-2-phenylpropanoate for 1-3 hours. For data
128 collection, crystals were transferred to cryoprotectant solutions consisting of mother liquor
129 plus 20-23% (v/v) glycerol before being cooled in liquid nitrogen. Diffraction data were
130 collected using synchrotron radiation on the XALOC beamline at ALBA (Cerdanyola del
131 Vallés, Spain). Diffraction images were processed with XDS [40] and merged using AIMLESS
132 [41] from the CCP4 package [42]. Both crystals were indexed in the C2 space group, with two
133 molecules in the asymmetric unit and 40% solvent content within the unit cell. The data
134 collection statistics are given in **Table S1**.

135

136 The structure of the complex was solved by difference Fourier synthesis using the
137 coordinates of the EH₃ native crystals (PDB ID: 6SXP). Crystallographic refinement was
138 performed using the program REFMAC [43] within the CCP4 suite with local
139 noncrystallographic symmetry (NCS). The free R-factor was calculated using a subset of 5%
140 randomly selected structure-factor amplitudes that were excluded from the automated
141 refinement. At the later stages, ligands were manually built into the electron density maps
142 with Coot [44], and water molecules were included in the model, which, when combined
with more rounds of restrained refinement, reached the R factors listed in **Table S1**. For

143 methyl-(*R/S*)-2-phenylpropanoate, which is not present in the Protein Data Bank, a model
144 was built using MacPyMOLX11Hybrid (the PyMOL Molecular Graphics System, Version 2.0,
145 Schrödinger, LLC). The model was used to automatically generate coordinates and molecular
146 topologies with eLBOW [45], which is suitable for REFMAC refinement. The figures were
147 generated with PyMOL. The crystallographic statistics of EH_{3S192A} complexed with methyl-
148 (*R/S*)-2-phenylpropanoate are listed in **Table S1**.

149

150 2.4. Site-directed mutagenesis

151 Mutagenic PCR was performed using the QuikChange Lightning Multi Site-Directed
152 Mutagenesis Kit (Agilent Technologies, Cheadle, UK), as described previously [22]. The
153 forward primers used to generate the EH_{3I244L} and EH_{3I244F} variants were as follows: 5'-
154 GCGAAAACAATGGCCTCATGATTGAACTGCATAAC-3' and 5'-
155 GCGAAAACAATGGCTTCATGATTGAACTGCATAAC-3', respectively. The pBXNH3 plasmid
156 containing EH₃ DNA [9] was used as a template to perform mutagenic PCR.

157

158 2.5. Hydrolytic activity assessment

159 Ester hydrolysis was assayed using a pH indicator assay in 384-well plates at 30°C and pH
160 8.0 in a Synergy HT Multi-Mode Microplate Reader in continuous mode at 550 nm over 24
161 hours. Conditions were as detailed previously [39]. For K_m determination, [protein]: 4.5 μg
162 ml^{-1} ; [ester]: 0-100 mM; reaction volume: 44 μl ; T: 30°C; and pH: 8.0. For k_{cat} determination,
163 [protein]: 0-270 μg ml^{-1} ; [ester]: 50 mM; reaction volume: 44 μl ; T: 30°C; and pH: 8.0.

164 The effect of pH on the activity was determined in 50 mM Britton and Robinson buffer
165 at pH 4.0–12.0, following the production of 4-nitrophenol from the hydrolysis of 4-
166 nitrophenyl-propionate ($p\text{NPC}_3$: 0.8 mM) at 348 nm ($\epsilon = 4147 \text{ M}^{-1} \text{ cm}^{-1}$) over 5 min and
167 determining the absorbance per minute from the slopes generated [22]. Reactions,
168 performed at 30°C, each contained 2 μg of protein in a total volume of 200 μl . Similar assay
169 conditions were used to assay the effects of temperature on esterase hydrolysis of $p\text{NPC}_3$,
170 but in this case, reactions were performed in 50 mM Britton and Robinson buffer pH 8.0.

171 All values, in triplicate, were corrected for nonenzymatic transformation. The absence of
172 activity was defined as at least a twofold background signal as described [39].

173

174 2.6. Hydrolysis of methyl-(*R/S*)-2-phenylpropanoate and gas chromatography (GC) analysis

175 Prior to the use of the racemic mixture, the continuous hydrolysis of separate methyl (*R*)-
176 2-phenylpropanoate and methyl (*S*)-2-phenylpropanoate was performed. Briefly, 2 μl of
177 each enantiomer (from a stock solution of 200 mg ml^{-1} in acetonitrile) was added to 96 μl of
178 5 mM 4-(2-hydroxyethyl)-1-piperazinepropanesulfonic acid (EPPS) buffer (pH 8.0) containing
179 0.9 mM Phenol Red (Merck Life Science S.L.U., Madrid, Spain). Then, 2 μl of enzyme solution
180 (from a stock solution of 1.0 mg ml^{-1} in 40 mM HEPES buffer, pH 7.0) was added, and the
181 progress of the reaction at 30°C was followed continuously at 590 nm. These reaction
182 conditions were set up to evaluate the chiral specificity using a racemic ester of methyl
183 (*R/S*)-2-phenylpropanoate. After 60 min, reactions with racemic mixtures were stopped by
184 adding 1800 μl of HPLC-grade methanol, and the reaction products were analyzed by GC
185 through a GC-Column CP-Chirasil-Dex CB (25 m length, 0.25 μm internal diameter, 0.25 μm
186 film) (Agilent J&W GC Columns), as previously described [22].

187

188 2.7. Circular dichroism to estimate the thermal denaturation of EH₃

189 Circular dichroism (CD) spectra were acquired between 190 and 270 nm with a Jasco J-
190 720 spectropolarimeter equipped with a Peltier temperature controller, employing a 0.1-mm
191 cell at 25°C. Spectra were analyzed, and denaturation temperature (T_d) values were
192 determined at 220 nm between 10 and 85°C at a rate of 30°C per hour in 50 mM Britton and
193 Robinson buffer at pH 8.5. A protein concentration of 1.0 mg ml⁻¹ was used. T_d (and standard
194 deviation of the linear fit) was calculated by fitting the ellipticity (mdeg) at 220 nm at each of
195 the different temperatures using a 5-parameter sigmoid fit with SigmaPlot 13.0.

196

197 *2.8. Cavity volume and solvent-accessible surface area (SASA) calculation*

198 The relative solvent-accessible surface area (SASA) of the active site, computed as a
199 (dimensionless) percentage of the ligand SASA in solution, was obtained using the GetArea
200 web server [46]. Note that the relative SASA of the catalytic triad (derived from the GetArea
201 server) adopts values of 0–100. The volume of the active site cavity was computed with
202 fpocket [47], which is a very fast open-source protein pocket (cavity) detection algorithm
203 based on Voronoi tessellation. fpocket includes two other programs (dpocket and tpocket)
204 that allow the extraction of pocket descriptors and the testing of owned scoring functions,
205 respectively.

206

207 *2.9. Evolutionary trace and evolutionary action computations*

208 The evolutionary importance of sequence positions was estimated using the *Evolutionary*
209 *Trace (ET) method* [36,37], which is available at <http://lichtargelab.org/software/ETserver>.
210 ET scores the functional importance of protein sequence positions by quantifying the
211 correlation of variations in homologous proteins with the phylogenetic divergence of the
212 sequences. Residue variations associated with large phylogenetic distances indicate
213 important residues, and vice versa. The ET output is given as a top-ranked score (on the
214 scale of 0 for the most important to 100 for the least important residues), which indicates
215 the percentage of protein residues that were found to be more important than the residue
216 of interest.

217 The functional impact of the potential amino acid substitutions was estimated using the
218 *Evolutionary Action (EA) method* [48], which is available at <http://eaction.lichtargelab.org/>.
219 EA estimates the evolutionary impact of sequence changes through a simple model of
220 protein evolution that accounts for the evolutionary importance of the residue (ET method)
221 and for the similarity of the substitution. The similarity of the substitution is quantified
222 through substitution odds that are specific to the evolutionary importance, secondary
223 structure, and solvent accessibility of each residue. The outcome is a rank score that
224 indicates the percentage of all potential amino acid changes in the protein that are predicted
225 to have less impact than the substitution of interest. Therefore, EA is given on a scale from 0
226 (fully neutral) to 100 (fully deleterious).

227 Both ET and EA are required as inputs to provide an alignment of homologous sequences.
228 We generated the input alignment using the default parameters of the ET server (UniRef90,
229 20% minimum sequence identity, 0.5 minimum fractional length to query), which resulted in
230 410 homologous sequences.

231

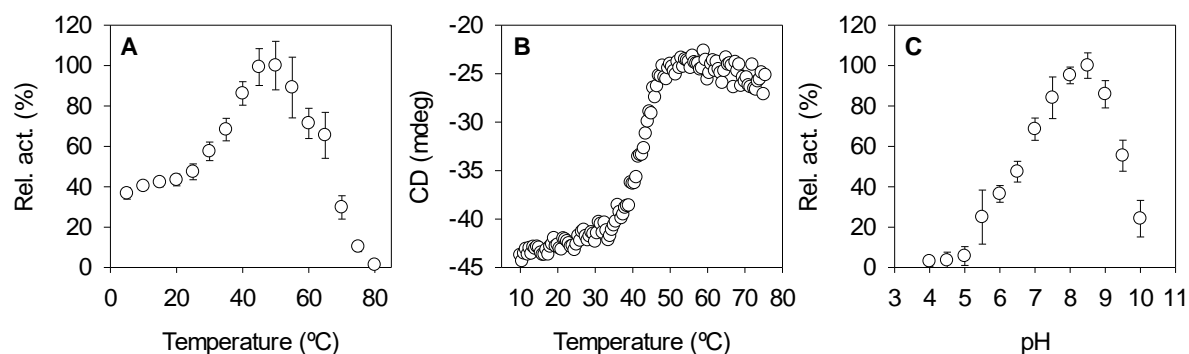
232 **3. Results and Discussion**

233

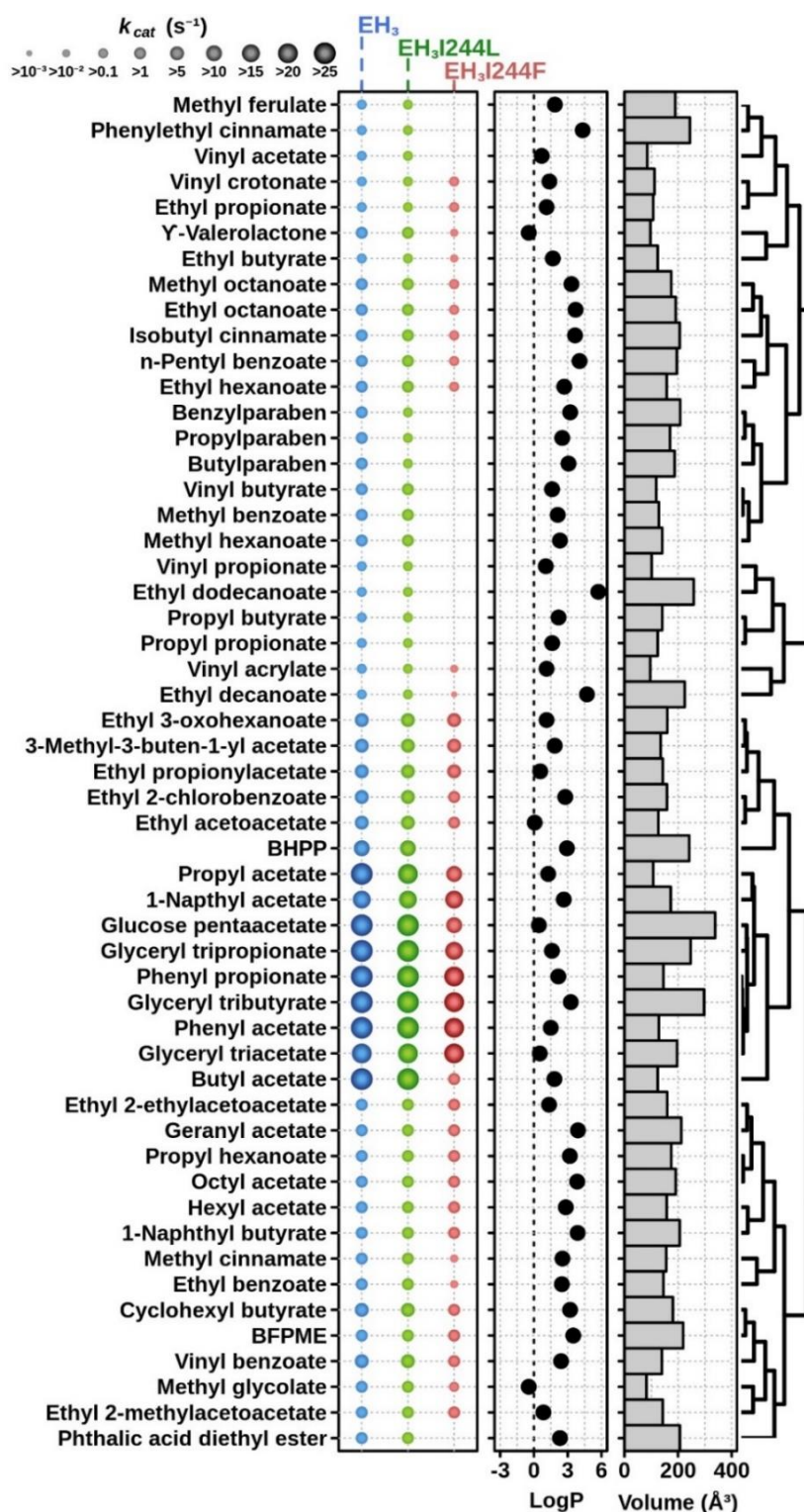
234 *3.1. Biochemical and substrate specificity characteristics of EH₃*

235 EH₃ was identified in a recent study as the third most substrate-ambiguous ester hydrolase
236 out of 145 tested enzymes [9]. This enzyme, which belongs to family IV of the Arpigny and
237 Jaeger classification [31], originated from an uncultured bacterium of the genus
238 *Hyphomonas* (phylum *Proteobacteria*), a highly versatile group of halophiles in terms of their
239 ability to successfully grow in a variety of environmental conditions and capable of
240 mineralizing a high number of pollutants [49]; this may be in agreement with the fact that
241 this enzyme was isolated from a chronically polluted seashore area [9].

242 EH₃ did show maximal activity at 50°C, retaining more than 80% of the maximum activity
243 at 40-55°C (**Fig. 1A**), suggesting that it is moderately thermostable. This was confirmed by
244 circular dichroism analysis, which revealed a denaturing temperature of $45.90 \pm 0.43^\circ\text{C}$ (**Fig.**
245 **1B**). Its optimal pH for activity is 8.5 (**Fig. 1C**). Its voluminous (volume of the active site
246 cavity: 1718.02 \AA^3) but low exposed (solvent accessible surface area (SASA): 6.03 over 100
247 dimensionless percentage) active site allows hydrolysis of a broad range of 71 structurally
248 and chemically diverse esters, including non-chiral (**Fig. 2**) and chiral (**Fig. 3**) esters. Such
249 topology, namely, active site cavities with large volume but low exposition to the surface,
250 has been found to be beneficial for retaining a higher number of substrates in specific
251 catalytic binding interactions and thus for promoting substrate promiscuity [9]. However, it
252 is not stereospecific according to the quick apparent enantioselectivity (E_{app}) method [50], in
253 which the ratios between the k_{cat}/K_m of the preferred chiral ester and the nonpreferred
254 chiral ester (from *ca.* 1.02 to 6.93; **Table 1**) were calculated when tested separately.

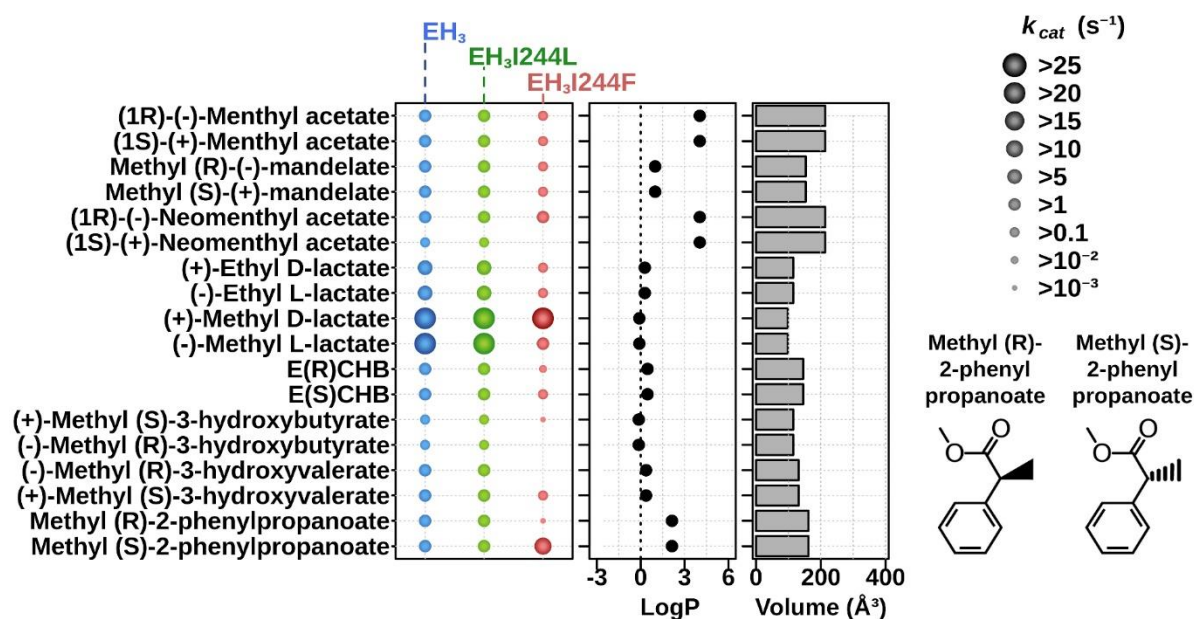


255 **Fig. 1.** Optimal parameters for the activity and stability of purified EH₃. (A) Temperature
256 profile determined as follows: protein, 2 μg ; [*p*-nitrophenyl propionate (*pNPC*₃)], 0.8 mM;
257 pH, 50 mM Britton and Robinson buffer pH 8.0; T, 5-80°C; reaction volume, 200 μl . (B) The
258 thermal denaturation curve of EH₃ at pH 7.0 was measured by ellipticity changes at 220 nm
259 and obtained at different temperatures. (C) The pH profile was determined as follows:
260 protein, 2 μg ; [*pNPC*₃], 0.8 mM; T, 30°C; pH, 50 mM Britton and Robinson buffer from 4.0 to
261 10.0; reaction volume, 200 μl . Graphics were created with SigmaPlot version 14.0. The data
262 are not fitted to any model.
263
264
265



266
 267 **Fig. 2.** Non-chiral substrate specificity. The k_{cat} (s^{-1}) values of the EH_3 , EH_{3I244L} and EH_{3I244F}
 268 variants were measured for 53 non-chiral carboxylic esters found to be hydrolyzed by any of
 269 the enzyme variants. The substrates, with the hydrophobicity (log P) and volume (\AA^3)
 270 indicated (details in **Table S2**), are ranked based on hierarchical clustering according to
 271 substrate similarity profiles. For k_{cat} determination, calculated on a continuous pH indicator
 272 assay, the conditions were as follows: [enzyme], 0-270 $\mu\text{g ml}^{-1}$; [ester], 50 mM to ensure
 273 substrate saturation; reaction volume, 44 μl ; T, 30°C; and pH, 8.0. Abbreviations are as
 274 follows: BFPME: benzoic acid, 4-formyl-, phenylmethyl ester; BHPP: benzyl (*R*)-2-hydroxy-3-

275 phenylpropanoate. LogP values and molecular volume of each ester were calculated using
 276 ACD/ChemSketch 2015.2.5 and Molinspiration software, respectively. For raw data and
 277 details, see Table S2.
 278



279
 280
 281 **Fig. 3.** Chiral substrate specificity. The k_{cat} (s⁻¹) values of the EH₃, EH₃I244L and EH₃I244F variants
 282 measured for 18 chiral carboxylic esters found to be hydrolyzed by any of the enzyme
 283 variants. Abbreviations are as follows: E(R)CHB, ethyl (R)-4-chloro-3-hydroxybutyrate;
 284 E(S)CHB, ethyl (S)-4-chloro-3-hydroxybutyrate. Figure preparation and experimental details
 285 are shown in Fig. 2. The structures of methyl-(R)-2-phenylpropanoate and methyl-(S)-
 286 phenylpropanoate used for soaking and investigation of chiral specificity are shown. LogP
 287 values and the molecular volume of each ester were calculated using ACD/ChemSketch
 288 2015.2.5 and Molinspiration software, respectively. For raw data and details, see Table S2.
 289

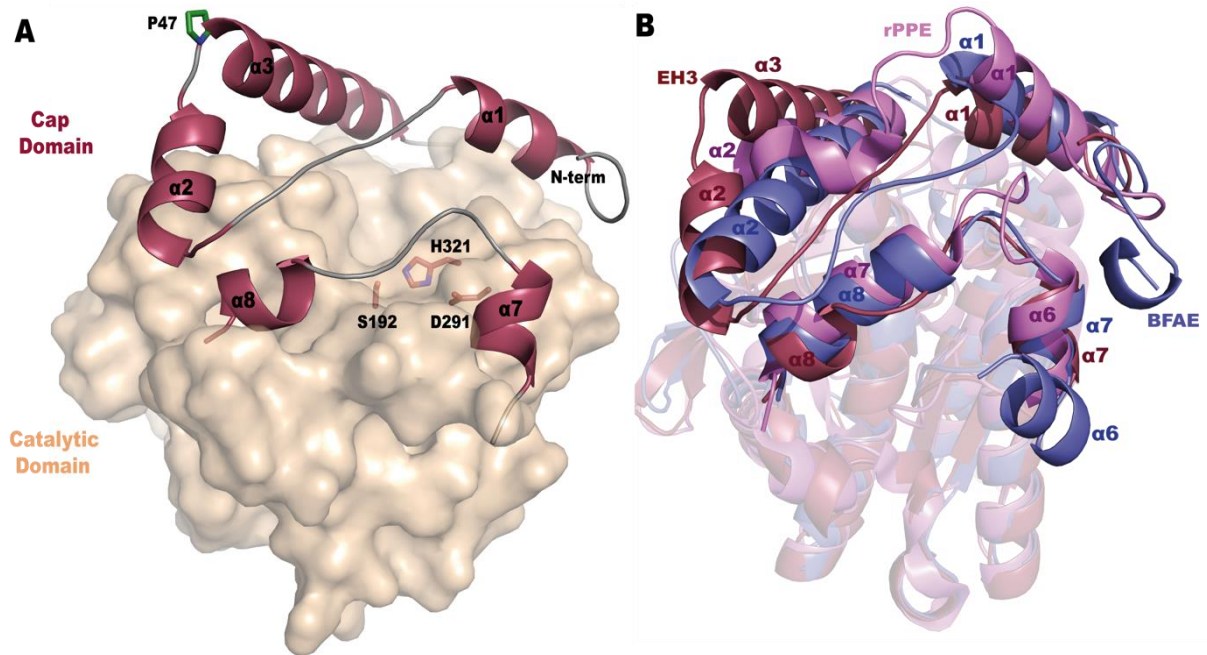
290 **Table 1.** E_{app} values for the hydrolysis of separate pairs of enantiomers.
 291

Chiral pair (R/S)	E_{app} : (k_{cat}/K_m preferred)/(k_{cat}/K_m nonpreferred) ¹		
	EH ₃	EH ₃ I244L	EH ₃ I244F
Menthyl acetate	1.71±0.25 (S)	1.50±0.39 (S)	6.40±0.37 (S)
Methyl mandelate	1.53±0.24 (S)	1.93±0.15 (S)	3.24±0.04 (S)
Neomenthyl acetate	6.93±0.35 (R)	6.88±0.14 (R)	100% specific (R)
Methyl lactate	2.35±0.11 (R)	2.49±0.03 (R)	226.5±4.5 (R)
Ethyl lactate	1.74±0.16 (R)	1.76±0.21 (R)	9.03±0.91 (R)
Ethyl-4-chloro-3-hydroxybutyrate	1.59±0.18 (R)	1.39±0.05 (R)	6.22±0.28 (R)
Methyl-3-hydroxybutyrate	1.33±0.34 (R)	1.27±0.16 (R)	100% specific (R)
Methyl-3-hydroxyvalerate	1.02±0.10 (R)	1.09±0.14 (R)	100% specific (R)
Methyl-2-phenylpropanoate	2.21±0.08 (S)	2.16±0.05 (S)	56300±42 (S)

292 ¹Calculated by following the hydrolysis of separate enantiomers in a continuous high-
 293 throughput pH indicator assay (see Materials and methods).
 294

295 3.2 Insights into the structural basis of EH₃ substrate ambiguity

296 As previously reported by us [39], the crystal structure of EH₃ showed that it is folded into
 297 two different domains: an α/β -hydrolase catalytic domain housing the catalytic triad (S192,
 298 A291, and H321) and a cap domain located on top and preventing the entrance of substrates
 299 into the active site (**Fig. 4A**). The polypeptide chain is folded into a total of eleven α -helices
 300 and eight β -sheets; five of the α -helices compose the cap domain, three at the N-terminus
 301 (α 1, α 2, α 3) and two more (α 7 and α 8) after strand β 6 from the central sheet (**Fig. S1**). The
 302 analysis of the B factor values revealed that the cap region comprising α 1- α 2 is highly
 303 flexible, with the loop linking both α -helices being partially disordered in the native structure
 304 but becoming more ordered upon substrate binding.
 305



306
 307
 308 **Fig. 4.** Crystal structure of EH₃. (A) Molecular surface of the catalytic domain (wheat) with
 309 the α -helices making up the cap domain depicted as a cartoon (plum); for secondary
 310 structure numbering, see **Fig. S1**. The catalytic triad is shown as sticks (orange). The region
 311 comprising α 1- α 2 is highly flexible, and P47 acts as a hinge (green sticks). (B)
 312 Superimposition of the EH₃ subunit (plum) and its homologues, BFAE (slate, PDB ID: 1JKM)
 313 and rPPE_{S159A/W187H} (violet, PDB ID: 4OB6). The cap domain presents the largest differences
 314 that configure markedly divergent active sites. The folding characteristics of Est22 and Est25
 315 are most similar to those of EH₃ and BFAE, respectively, and have been omitted for clarity.
 316

317 To disclose the molecular basis behind the substrate ambiguity, we compared the EH₃
 318 structure with other reported esterases. As expected, this highly flexible cap is the most
 319 variable region among homologues. Analysis of EH₃ folding using the *DALI* server shows that
 320 its closest homologue is Est22, which was isolated from environmental samples, with 64%
 321 identity and an RMSD of 0.9 Å from 336 C α atoms [51] (PDB ID: 5HC0). Other homologues
 322 are Est25 from environmental samples (RMSD of 1.8 Å from 323 C α atoms, PDB ID: 4J7A
 323 [52]), Brefeldin A (BFAE) from *Bacillus subtilis* (RMSD of 2.0 Å from 323 C α atoms, PDB ID:
 324 1JKM [53]) and the carboxylesterase rPPE from *Pseudomonas putida* (RMSD of 2.0 Å from
 325 297 C α atoms, PDB ID: 4OB6 [54]), and these three proteins are 20-40% identical to EH₃.
 326 They all belong to the hormone-sensitive lipase (HSL) family or family IV [31]. This HSL family

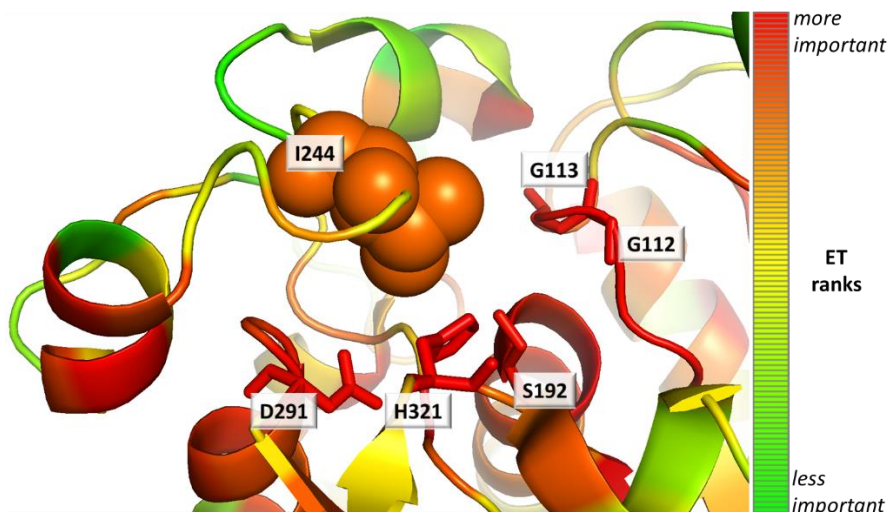
327 presents a very conserved folding at the core α/β domain, with the largest differences at the
328 cap domain that, consequently, must be mostly responsible for their different functionalities
329 (**Fig. 4B**). First, the loop connecting helices $\alpha 1$ and $\alpha 2$ is very short in rPPE, and as a result,
330 the active site cavity of this protein is reduced, allowing relatively small substrates to enter.
331 Moreover, the EH₃ and Est22 $\alpha 2$ and $\alpha 3$ helices are fused into a unique long α -helix in BFAE
332 and Est25. Although this arrangement in two separate, more mobile helices is shared with
333 Est22, EH₃ presents a proline residue at the beginning of $\alpha 3$ (P47, but this residue is a
334 glutamate in Est22), which could act as a hinge to increase the mobility of the EH₃ $\alpha 1$ - $\alpha 2$
335 moiety (**Fig. 4A**). This feature might be an additional mechanism that adapts the topology of
336 the EH₃ active site to a higher variety of substrates and explains its observed substrate
337 promiscuity. Furthermore, the shorter $\alpha 8$ in EH₃ makes a longer $\alpha 7$ - $\alpha 8$ loop and a wider
338 catalytic site, probably also contributing to the superior substrate promiscuity of EH₃.
339 Moreover, as a homologous HSL enzyme, EH₃ is a homodimer where both subunits are
340 related by a twofold symmetry axis (**Fig. S2, Table S3**).

341 To conclude, EH₃ may be considered a moderately thermostable serine ester hydrolase
342 with prominent substrate ambiguity but is not stereospecific. This is the result of its novel
343 capacity to adapt the topology of the large but occluded active site to a high variety of
344 substrates.

346 3.3. Evolutionary screening of specificity swapping positions

347 To explore the functional roles of sequence positions, we used the Evolutionary Trace (ET)
348 method [36,37]. In previous work [38], ET identified few key sequence positions that were
349 able to alter the substrate specificity of homologous proteins; therefore, we hypothesized
350 that ET would also be able to identify positions that modulate enzyme specificity in
351 combination with substrate promiscuity. According to the ET ranks for the EH₃ protein
352 (shown in **Table S4**), position 244 was ranked within the top 12% of residues, and it is the
353 most important residue of the loop formed by residues 240-249 (loop $\alpha 7$ - $\alpha 8$ at the cap, **Fig.**
354 **4A**), which are in contact with the catalytic triad (**Fig. 5**).

355



356

357 **Fig. 5.** Evolutionary trace ranks for the EH₃ protein. The analysis used 410 homologous
358 sequences of EH₃ with sequence identity as low as 20%. The ET ranks are represented on the
359 structure with a color scale (the most important residues are red, and the least important
360 residues are green). While the catalytic residues were ranked within the top most important
361 residues (S192 was 3%, D291 was 2%, and H321 was 1%), residue I244 was ranked in the top

362 12%, and it was the most important residue of loop 240-249 in contact with the catalytic
 363 residues. The figure was generated using the PDB structure 6SXP, PyMOL (version 1.8), ET
 364 (with the position-specific option), and the PyMOL ET viewer [55].
 365

366 Leucine and isoleucine are amino acids that are most commonly present (*ca.* 70% of the
 367 closest homologous sequences) at position 244, as shown in the alignment, while other
 368 amino acids, such as tryptophan and valine, appear less frequently and mostly in distant
 369 homologs (**Table 2**). This was also confirmed when we used BLAST to search for the EH₃
 370 sequence in the nonredundant (nr) [56], UniProt [57], and Marref, MarDB and MarCat [58]
 371 databases. We were able to report up to 10,000 alignment hits with a minimum query
 372 coverage of 50% and an e-value cutoff of 1e⁻¹⁰, ensuring in all cases the correct alignment of
 373 the three residues forming the catalytic triad (S192, D291, and H321), the two residues
 374 (G112 and G113) forming the so-called oxyanion hole-stabilizing substrates, and the residue
 375 (P47) acting as a hinge that allows mobility of the cap domain to control substrate access to
 376 the catalytic site. Above an identity of 50%, all homologues contain either isoleucine (top
 377 homologue WP_156780860.1; identify, 67%; e-value, 3e⁻¹⁷⁶) or leucine (top homologue
 378 AKJ87259.1; identify, 66%; e-value, 7e⁻¹⁶⁸), while TNF86759.1 (identify 67%; e-value 3e⁻¹⁶⁹)
 379 contains a methionine, and E3QWZ9 (identify 35%; e-value 2e⁻⁴⁵) contains a phenylalanine
 380 (**Table 2**). Variability at this position was only found to a higher extent at identities below
 381 39.38% and e-values above 2.62 × 10⁻⁶⁹ (**Table 2**).
 382

383 **Table 2.** Frequency of amino acids at position I244 (following EH₃ numeration) in EH₃-
 384 homologous proteins as detected by ET analysis and the top homologs.
 385

AA at 244 ¹	Frequency (%) ¹	Top homologs		
		Accession number	Identity (%)	E-value
L	63.08	AKJ87259.1 ²	66.00	7.00 × 10 ⁻¹⁶⁸
W	19.56	MBE82488.1 ³	32.49	1.32 × 10 ⁻³⁰
I	8.07	WP_156780860.1 ²	67.00	3.00 × 10 ⁻¹⁷⁶
V	3.18	HAY66678.1 ³	40.78	8.13 × 10 ⁻⁶⁶
N	2.20	WP_042512518.1_MMP04251492 ³	31.35	2.80 × 10 ⁻²³
T	0.98	GCA_002427755.1 ³	32.18	5.84 × 10 ⁻³¹
F	0.73	E3QWZ9 ¹	35.00	2.00 × 10 ⁻⁴⁵
A	0.49	WP_073577520.1 ³	33.42	5.14 × 10 ⁻⁵³
H	0.49	POP51947.1_MMP08281192 ³	31.23	1.34 × 10 ⁻²¹
M	0.49	TNF86759.1 ²	67.00	3.00 × 10 ⁻¹⁶⁹
G	0.24	MMP491463_308377 ³	38.18	2.47 × 10 ⁻⁵⁶
P	0.24	WP_071722916.1_MMP05231544 ³	30.15	6.93 × 10 ⁻²³
S	0.24	GCA_002389675.1 ³	32.05	4.22 × 10 ⁻²⁷

386 ¹As a default, the server uses the UniRef90 database. This database was created after
 387 filtering out sequences so that it does not contain duplicates or similar sequences (higher
 388 sequence identity than 90%) among its members. This makes it a good source to find "more
 389 representative" full-length sequences (fragments and short sequences were removed) of the
 390 protein family evolution and indeed results in better ET accuracy than using more sequences
 391 from other databases. The BLAST option for sequence identity was 20% (min.) to 95% (max.).
 392 The e-value cutoff was 0.05, and up to 500 sequences were selected (above this number of

393 representative sequences, the ET scores no longer improved). Based on these results, the
394 different amino acids (AAs) found at position 244 (following EH₃ numbering) are given.

395 ²nr database (<https://blast.ncbi.nlm.nih.gov>)

396 ³Other databases: UniProt (<https://www.uniprot.org/>) and MAR

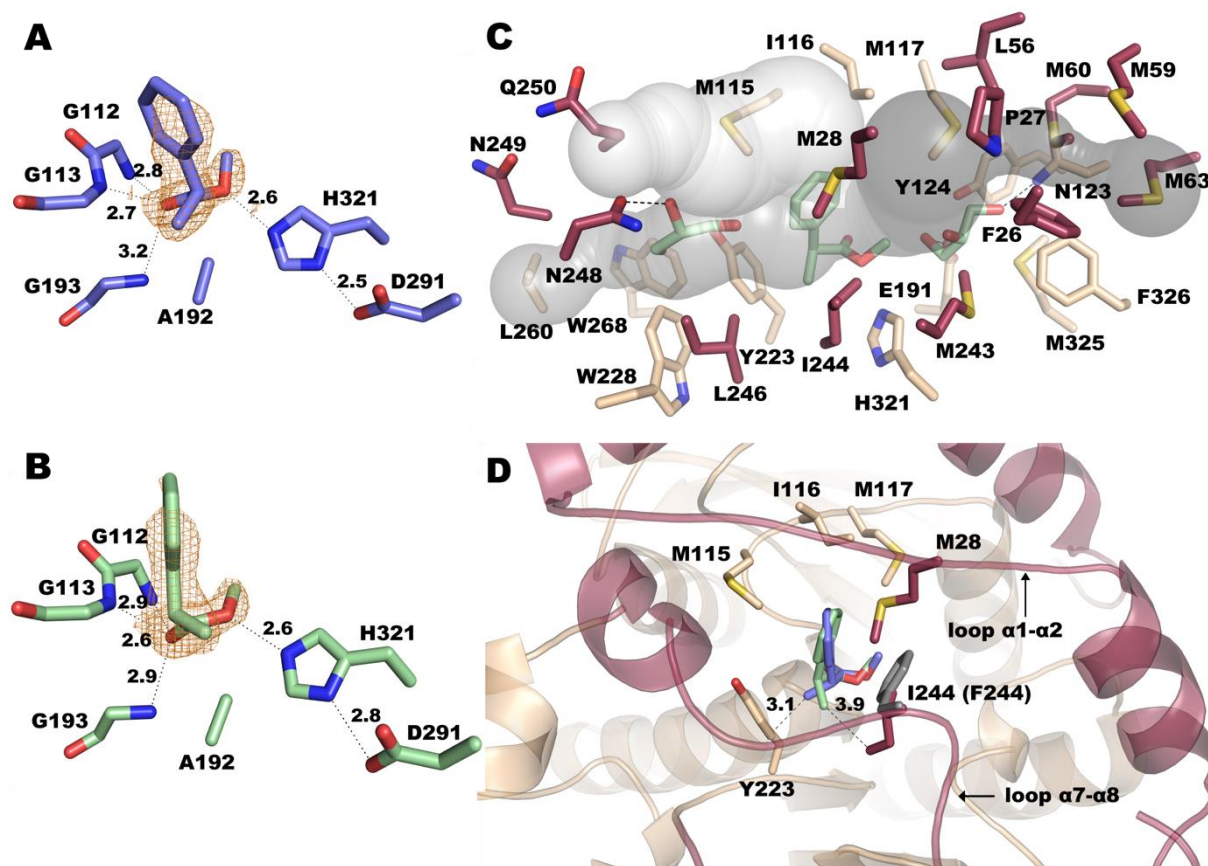
397 (<https://mmp.sfb.uit.no/blast/>).

398

399 3.4. Crystal structure of the substrate-bound form of EH₃ to determine the functional role of 400 I244

401 Our evolutionary trace analysis suggested that a single residue at position 244 potentially
402 had a functionally important role in EH₃. Soaking of inactivated EH_{3S192A} crystals in a solution
403 containing either methyl-(*R*)-2-phenylpropanoate or methyl-(*S*)-2-phenylpropanoate was
404 performed in this study to further investigate whether I244, or other amino acid residue(s) if
405 any, is close to the substrate's stereo-center and plays a functional role in specificity, as
406 suggested by ET analysis. This chiral ester was selected as a model because it is structurally
407 similar to ibuprofen-like esters that are of great industrial relevance, and the wild-type
408 enzyme showed a lack of specificity for these chiral esters based on the E_{app} value (**Table 1**).
409 The crystal structures of these complexes were solved using the coordinates of wild-type EH₃
410 (PDB ID: 6SXP). The final models were refined to crystallographic R-factors of 0.2100 and
411 0.1919 and R-free values of 0.2403 and 0.2276 with resolutions of 2.27 and 2.06 Å (PDB IDs:
412 6SYA and 6SXY), respectively. Both crystals present two molecules in the asymmetric unit
413 forming the dimer and one ligand bound per catalytic site (**Figs. 6A and 6B**).

414



415

416

417 **Fig. 6.** Active site of EH₃. (A) Methyl (*2R*)-2-phenylpropanoate and (B) methyl (*2S*)-2-
418 phenylpropanoate bound at the catalytic site of EH_{3S192A}, showing that the 2Fo-Fc electron

419 density maps contoured at 0.9 and 0.8 σ are in orange. (C) Active site channels of EH_{3S192A}, as
420 calculated by CAVER [59], with bound methyl (2S)-2-phenylpropanoate and two glycerol
421 molecules. The residues surrounding each cavity are shown. (D) Nearest environment and
422 conserved binding mode of methyl (2R)-2-phenylpropanoate (slate) and methyl (2S)-2-
423 phenylpropanoate (pale green) in the complexes; the closest distance from each substrate to
424 the EH₃ residue is shown. The putative position of the modeled I244F mutant is shown as
425 gray sticks. Panels C and D show the same color code as Fig. 4A.
426

427 The catalytic triad of EH₃ is formed by S192, D291 and H321. There are three conserved
428 motifs in its sequence, ¹¹⁰HGGG¹¹³ (containing two of the glycines involved in the oxyanion
429 hole), the pentapeptide ¹⁹⁰GXSXG¹⁹⁴ (housing the nucleophile serine and a third glycine) and
430 ²⁹¹DPLRDEG²⁹⁷ (including D291). The substrates are bound by polar interactions of its free
431 carboxylate oxygen with the three glycines forming the oxyanion hole and hydrogen bonds
432 of the ester oxygen to H321 from the catalytic triad (Figs. 6A and 6B). Structural
433 superimposition of the wild-type coordinates with the complexes presented here shows no
434 structural changes in the EH₃ active site upon complex formation, and both complexes
435 maintain high B factor values for the cap domain. As we previously described, the EH₃ active
436 site cavity possesses three long channels giving access to catalytic S192, an acyl binding site
437 (approximately 11.2 Å), an alcohol binding site (10.9 Å) and a third channel that can possibly
438 allocate substrates with branched acyls (Fig. 6C). In the complex reported here, the acyl
439 channel is partially occupied by phenyl/methyl rings, whereas the alcohol binding channel is
440 allocated to a small aliphatic group (methyl). Chain B from both complexes also
441 accommodates two molecules of glycerol coming from the cryoprotectant, one at the acyl
442 moiety and the other at the alcohol site. As seen in Fig. 6C, all three channels are shaped by
443 mostly hydrophobic residues from the cap and the catalytic domains that, in principle, would
444 not present specific interactions with the substrates, explaining the EH₃ promiscuity and
445 absence of stereospecificity. Thus, residues M115, Y223, W228, L246, I244 and L260
446 protrude at the acyl channel, making a mostly hydrophobic tunnel where only N248 seems
447 able to make polar interactions with the trapped glycerol molecule. In the alcohol channel,
448 hydrophobic residues F26, L56, M59, M60 and M63 emerge, among others, and only two
449 polar residues, N123 and E191, form hydrogen bonds with the glycerol trapped within this
450 channel.

451 A close inspection of the substrate complexes reveals the main features of the binding
452 modes of both isomers (Fig. 6D). Keeping the same polar interactions at the carboxylate
453 ester moiety shown in Figs. 6A and 6B, the orientation of their bulky phenyl ring is slightly
454 adjusted in a hydrophobic pocket surrounded by M115-I116-M117 from the catalytic
455 domain and M28 from the cap α 1- α 2 loop. The position of the aromatic ring is tilted in this
456 pocket in the proper way that minimizes the steric hindrance of the methyl group to the
457 closest residues, Y223 (in the *R* isomer) or I244 (in the *S* isomer), both delineating the
458 proximal region of the acyl channel. Therefore, in principle, these two positions may be
459 potential candidates to introduce the binding preferences of the isomers. However, changes
460 in Y223, which is tightly fixed by the interaction with W228 and W268, as seen in Fig. 6C,
461 might be deleterious for the active site integrity. This, together with the fact that Y223 was
462 found to be less important than I244 (cap domain) according to evolutionary traces (most
463 important 32%), similar to its interacting tryptophans (W228 and W268 were most
464 important 57% and 22%, respectively), was the basis by which we concentrated our efforts

465 on I244. Its close proximity to the substrates and its prominent position at the long $\alpha 7$ - $\alpha 8$
466 loop suggest a crucial role in binding specificity.

467 To conclude, our structural analysis of the chiral substrate-bound form of inactivated
468 protein has provided new information explaining the broad substrate promiscuity of EH₃,
469 which could not be observed previously by examining the crystal structure in free form [39].
470 Indeed, the results imply that three long channels exist and give access to the catalytic
471 nucleophile, which may then also contribute to the prominent substrate ambiguity of EH₃
472 and to its capacity to accept a large variety of esters with different sizes and degrees of
473 conformational dynamics without chiral specificity. In addition, it has also contributed to
474 confirming position 244 as a key position possibly influencing chiral specificity, thus
475 supporting ET prediction.

476 477 *3.5. Position 244 introduces chiral specificity without major influences on substrate* 478 *ambiguity*

479 To choose which amino acid substitutions of residue I244 to study experimentally, in
480 addition to evolutionary trace analysis, BLAST and structure analyses, we used the
481 Evolutionary Action (EA) method. EA estimates the functional impact of each mutation in a
482 protein and ranks the variants on a scale from 0 (fully neutral) to 100 (fully deleterious) [48],
483 while variants with intermediate scores (e.g., between 40 and 70) have been linked with the
484 partial loss or gain of function. In search of gain-of-function effects, we decided to perform
485 two mutations: I244L, which has an EA score of 47 and appears in many homologous
486 sequences (identity up to 66%), and I244F, which is a large amino acid, has an EA score of *ca.*
487 64, and appears only in distant homologs (E3QWZ9-1, 35% identity as top hit) (**Table 3**).

488
489 **Table 3. EA scores for mutations in position I244 of EH₃.**
490

Substitution	Evolutionary Action
I244V	37.83
I244L	46.94
I244M	47.51
I244F	63.58
I244Y	75.39
I244C	75.51
I244T	75.83
I244A	80.26
I244W	81.50
I244N	88.04
I244S	88.93
I244Q	89.28
I244P	89.47
I244H	90.50
I244R	92.53
I244G	93.95
I244K	95.10
I244E	96.97
I244D	97.55

491

492 The EH_{3I244L} and EH_{3I244F} variants were created by site-directed mutagenesis, and after
493 expression in the pBXNH3 plasmid and *E. coli* MC1061 cells, the mutants were expressed,
494 purified and characterized using the same protocols as those for the wild-type hydrolase
495 following the hydrolysis of 98 carboxylic ester substrates. Their overall substrate spectra,
496 maximum conversion rates and preferences for chiral esters were evaluated and compared
497 with those of the wild-type protein.

498 As shown in **Figs. 2** and **3**, EH₃ can transform as many as 71 substrates, including chiral
499 and non-chiral substrates, with the highest k_{cat} of 1730.3 min⁻¹; these features were also
500 characteristic of the EH_{3I244L} mutant capable of hydrolyzing the same set of substrates (**Figs.**
501 **2** and **3**) at similar rates (highest k_{cat} of 1731.3 min⁻¹); indeed, the differences in k_{cat} for the
502 conversion of each ester ranged only from *ca.* 0.7- to 3.2-fold, which suggests no major
503 effects of the mutation on the substrate specificity and conversion rate. The substrate
504 spectrum of EH_{3I244F} was slightly reduced to 53 substrates (**Figs. 2** and **3**); many large
505 substrates could not be hydrolyzed (such as long alkyl esters or paraben esters), but small
506 substrates such as vinyl acetate and butyrate or propyl propionate and butyrate could be
507 hydrolyzed. Furthermore, when compared to those of the wild type, the k_{cat} values of
508 EH_{3I244F} appeared to be lower for most substrates converted, with an average reduction of
509 *ca.* 2.21 (interquartile range from 9.35 to 1.24) and a maximal reduction up to 992-fold (for
510 methyl (*R*)-2-phenylpropanoate). Conversion only increased by *ca.* 2.9-fold for methyl (*S*)-2-
511 phenylpropanoate. These reductions in the substrate repertoire and the conversion rate can
512 be reasonably attributed to the incorporation of a large amino acid residue that does not
513 accommodate as many substrates as wild-type EH₃ and mutant EH_{3I244L}.

514 Strikingly, the analysis of the k_{cat} values of separate enantiomers within a series of nine
515 chiral ester couples further revealed significant differences in the preference for chiral esters
516 (**Fig. 3**). This is exemplified by the apparent significant preference of the EH_{3I244F} mutant for
517 methyl (*S*)-2-phenylpropanoate, (1*R*)-neomethyl acetate, methyl (*S*)-3-hydroxybutyrate, and
518 methyl (*S*)-3-hydroxyvalerate compared to their chiral partners. This contrasts with the wild-
519 type EH₃ and the EH_{3I244L} mutant, which display no apparent preference for any of the chiral
520 pairs (**Fig. 3**). As shown in **Table 1**, the E_{app} values of EH₃ and mutant EH_{3I244L} ranged from
521 1.02±0.10 to 6.93±0.35 and from 1.04±0.14 to 6.88±0.14, respectively. In contrast, EH_{3I244F}
522 hydrolyzed (1*R*)-neomethyl acetate, methyl (*S*)-3-hydroxybutyrate, and methyl (*S*)-3-
523 hydroxyvalerate, with no appreciable hydrolysis of the other enantiomers detected with our
524 assay conditions, and showed high preferences for methyl (*R*)-lactate (E_{app} : *ca.* 227±5) and
525 methyl-(*S*)-2-phenylpropanoate (E_{app} : *ca.* 56300±42) (**Table 1**); these values are above $E_{app} >$
526 25, indicative of interest for industrial applications [39].

527 Encouraged by these promising results, we carried out additional kinetic analyses with
528 separate methyl-2-propanoate enantiomers used for soaking experiments and confirmed
529 the absence of preferences of EH₃ and EH_{3I244L} at any incubation time (**Fig. S3**) and the
530 marked preference of EH_{3I244F} for methyl-(*S*)-2-phenylpropanoate. These results were
531 confirmed by measuring the enantiomeric excess (*e.e.*%) with a racemic mixture of methyl-2-
532 propanoate enantiomers by GC [22], with values of 99.99±0.35% for EH_{3I244F}, 41.70±0.48%
533 for EH₃ and 42.5±0.44% for EH_{3I244L}.

534 Collectively, EH₃ gained stereospecificity properties in the I244F mutant. This increase can
535 be explained by the presence of a bulky residue that impedes the binding or positioning of
536 one of the enantiomers. In the case of the methyl-2-phenylpropanoate substrate, for
537 instance, both isomers could be able, in principle, to properly stack their phenyl moiety
538 against the aromatic F244 side chain (**Fig. 6D**), but then the (*R*) isomer would probably

539 present high steric hindrance of its methyl group to the Y223 side chain, resulting in a
540 preference for methyl-(*S*)-2-phenylpropanoate binding.

541

542 **4. Conclusions**

543 Although multiple lines of evidence indicate a general trend of enzymes evolving from a
544 generalist ancestor that accepts a broad range of substrates to a specialist enzyme [4], to
545 our knowledge, there is no information on the coevolution of multi-specificity and chiral
546 specificity. Here, combined analyses of specificity through evolutionary trace, structure
547 determination and mutagenesis reveal that substrate ambiguity and chiral specificity in a
548 single hydrolase can be modulated by a single residue. In this way, it is feasible to engineer
549 prominent substrate-promiscuous yet stereospecific hydrolases that are relevant to the field
550 of organic synthesis. We hypothesize that the number of enzymes with such characteristics
551 will increase in the future through screening evolutionarily important single sequence
552 positions, allowing us to swap substrate ambiguity and chiral specificity.

553

554 **5. Accession number**

555 The coordinates and structure factors of EH_{3S192A} complexed with methyl-(*R/S*)-2-
556 phenylpropanoate have been deposited in the Protein Data Bank with the accession codes
557 6SYA and 6SXY.

558

559 **CRedit authorship contribution statement**

560 **Isabel Cea-Rama:** Methodology, Formal analysis. **Cristina Coscolín:** Methodology, Formal
561 analysis. **Panagiotis Katsonis:** Methodology, Formal analysis. **Rafael Bargiela:** Formal
562 analysis. **Peter N. Golyshin:** Methodology, Funding acquisition. **Olivier Lichtarge:**
563 Methodology, Funding acquisition. **Manuel Ferrer:** Formal analysis, Resources, Writing –
564 original draft, Funding acquisition. **Julia Sanz-Aparicio:** Formal analysis, Resources, Writing –
565 original draft, Funding acquisition.

566

567 **Declaration of Competing Interests**

568 The authors declare that they have no known competing financial interests or personal
569 relationships that could have appeared to influence the work reported in this paper.

570

571 **Acknowledgments**

572 MF acknowledges the grant 'INMARE' from the European Union's Horizon 2020 (grant
573 agreement no. 634486), the grants PCIN-2017-078 (within the Marine Biotechnology ERA-
574 NET) and BIO2017-85522-R from the Ministerio de Economía, Industria y Competitividad,
575 Agencia Estatal de Investigación (AEI), Fondo Europeo de Desarrollo Regional (FEDER) and
576 the European Union (EU), and the grant 2020AEP061 from the Agencia Estatal CSIC. J.S.-A.
577 acknowledges grant PID2019-105838RB-C33 from the Ministerio de Ciencia e Innovación,
578 Agencia Estatal de Investigación (AEI), Fondo Europeo de Desarrollo Regional (FEDER) and
579 the European Union (EU). P.N.G. acknowledges the support of the Era-Net IB Project
580 MetaCat funded through UK Biotechnology and Biological Sciences Research Council
581 (BBSRC), grant No. BB/M029085/1, and the Centre for Environmental Biotechnology Project,
582 co-funded by European Regional Development Fund (ERDF) via the Welsh Government
583 (WEFO); R.B. acknowledges the Supercomputing Wales project, co-funded by ERDF via
584 WEFO. OL and PK were supported by the National Institutes of Health (NIH) grants
585 5R01AG061105, 5R01GM066099, and 5R01GM079656. C. Coscolín thanks the Ministerio de

586 Economía y Competitividad and FEDER for a PhD fellowship (Grant BES-2015-073829). The
587 authors would like to acknowledge David Rojo and Coral Barbas for GC analyses and David
588 Almendral and Ruth Matesanz for CD analyses. We thank the staff of the Synchrotron
589 Radiation Source at Alba (Barcelona, Spain) for assistance at the BL13-XALOC beamline.

590

591 **Appendix A. Supplementary data**

592 Supplementary data for this article can be found online.

593

594 **References**

595

- 596 [1] Jegannathan KR, Nielsen PH (2013) Environmental assessment of enzyme use in industrial
597 production – a literature review. *J Clean Prod* 42: 228-240.
- 598 [2] Sheldon RA, Woodley JM (2018) Role of biocatalysis in sustainable chemistry. *Chem Rev* 118:
599 801-838.
- 600 [3] Ferrer M, Méndez-García C, Bargiela R, Chow J, Alonso S, et al. (2020) Decoding the ocean's
601 microbiological secrets for marine enzyme biodiscovery. *FEMS Microbiol Lett* 366: fny285.
- 602 [4] Tawfik DS, Gruic-Sovulj I (2020). How evolution shapes enzyme selectivity - lessons from
603 aminoacyl-tRNA synthetases and other amino acid utilizing enzymes. *FEBS J* 287: 1284-1305.
- 604 [5] Coscolín C, Martínez-Martínez M, Chow J, Bargiela R, García-Moyano A, et al. (2018)
605 Relationships between substrate promiscuity and chiral selectivity of esterases from
606 phylogenetically and environmentally diverse microorganisms. *Catalysts* 8: 10.
- 607 [6] Arnold FH (2019) Innovation by evolution: Bringing new chemistry to life (Nobel lecture). *Angew*
608 *Chem Int Ed Engl* 58: 14420-14426.
- 609 [7] Suplatov D, Švedas V (2015) Study of functional and allosteric sites in protein superfamilies. *Acta*
610 *Naturae* 7: 34-45.
- 611 [8] Berezovsky IN, Guarnera E, Zheng Z, Eisenhaber B, Eisenhaber F (2017) Protein function
612 machinery: from basic structural units to modulation of activity. *Curr Opin Struct Biol* 42: 67-74.
- 613 [9] Martínez-Martínez M, Coscolín C, Santiago G, Chow J, Stogios PJ, et al. (2018) Determinants and
614 Prediction of Esterase Substrate Promiscuity Patterns. *ACS Chem Biol* 13: 225-234.
- 615 [10] Alcaide M, Tornés J, Stogios, PJ, Xu X, Gertler C, et al. (2013) Single residues dictate the co-
616 evolution of dual esterases: MCP hydrolases from the α/β hydrolase family. *Biochem J* 454: 157-
617 166.
- 618 [11] Cadet F, Fontaine N, Li G, Sanchis J, Ng Fuk Chong M, et al. (2028) A machine learning approach
619 for reliable prediction of amino acid interactions and its application in the directed evolution of
620 enantioselective enzymes. *Sci Rep* 8: 16757.
- 621 [12] Koudelakova T, Chovancova E, Brezovsky J, Monincova M, Fortova A, et al. (2011) Substrate
622 specificity of haloalkane dehalogenases. *Biochem J* 435: 345-354.
- 623 [13] Purg M, Pabis A, Baier F, Tokuriki N, Jackson C, Kamerlin SC (2016) Probing the mechanisms for
624 the selectivity and promiscuity of methyl parathion hydrolase. *Philos Trans A Math Phys Eng Sci*
625 374: 20160150.
- 626 [14] Ramírez-Escudero M, Del Pozo MV, Marín-Navarro J, González B, Golyshin PN, et al. (2016)
627 Structural and functional characterization of a ruminal β -glycosidase defines a novel subfamily
628 of glycoside hydrolase family 3 with permuted domain topology. *J Biol Chem* 291: 24200-24214.
- 629 [15] Albesa-Jové D, Guerin ME (2016) The conformational plasticity of glycosyltransferases. *Curr Opin*
630 *Struct Biol* 40: 23-32.
- 631 [16] Garrabou X, Macdonald DS, Wicky BIM, Hilvert D (2018) Stereodivergent evolution of artificial
632 enzymes for the michael reaction. *Angew Chem Int Ed Engl* 57: 5288-5291.
- 633 [17] Ekroos M, Sjögren T (2006) Structural basis for ligand promiscuity in cytochrome P450 3A4. *Proc*
634 *Natl Acad Sci USA* 103: 13682-13687.

- 635 [18] Zou T, Risso VA, Gavira JA, Sanchez-Ruiz JM, Ozkan SB (2015) Evolution of conformational
636 dynamics determines the conversion of a promiscuous generalist into a specialist enzyme. *Mol*
637 *Biol Evol* 32: 132-143.
- 638 [19] Gao S, Zhu S, Huang R, Li H, Wang H, Zheng G (2017) Engineering the enantio-selectivity and
639 thermostability of a (+)- γ -lactamase from *Microbacterium hydrocarbonoxydans* for kinetic
640 resolution of vince lactam (2-azabicyclo[2.2.1]hept-5-en-3-one). *Appl Environ Microbiol* 84:
641 e01780-17.
- 642 [20] Mateljak I, Monza E, Lucas MF, Guallar V, Aleksejeva O, et al. (2019) Increasing redox potential,
643 redox mediator activity and stability in a fungal laccase by computer-guided mutagenesis and
644 directed evolution. *ACS Catal* 9: 4561-4572.
- 645 [21] Wu Z, Kan SBJ, Lewis RD, Wittmann BJ, Arnold FH (2019) Machine learning-assisted directed
646 protein evolution with combinatorial libraries. *Proc Natl Acad Sci USA* 116: 8852-8858.
- 647 [22] Alonso S, Santiago G, Cea-Rama I, Fernandez-Lopez L, Coscolín C, et al. (2020) Genetically
648 engineered proteins with two active sites for enhanced biocatalysis and synergistic chemo- and
649 biocatalysis. *Nat Catal* 3: 319-328.
- 650 [23] Park S, Morley KL, Horsman GP, Holmquist M, Hult K, et al. (2005) Focusing mutations into the P.
651 fluorescens esterase binding site increases enantioselectivity more effectively than distant
652 mutations. *Chem Biol* 12: 45-54.
- 653 [24] Lafaquière V, Barbe S, Puech-Guenot S, Guieysse D, Cortés J, et al. (2009) Control of lipase
654 enantio-selectivity by engineering the substrate binding site and access channel. *Chembiochem*
655 10: 2760-2771.
- 656 [25] Antipov E, Cho AE, Klivanov AM (2009) How a single-point mutation in horseradish peroxidase
657 markedly enhances enantioselectivity. *J Am Chem Soc* 131: 11155-11160.
- 658 [26] Sevrioukova IF, Poulos TL (2013). Understanding the mechanism of cytochrome P450 3A4:
659 recent advances and remaining problems. *Dalton Trans* 42: 3116-3126.
- 660 [27] Stenner R, Steventon JW, Seddon A, Anderson JLR (2020) A de novo peroxidase is also a
661 promiscuous yet stereoselective carbene transferase. *Proc Natl Acad Sci USA* 117: 1419-1428.
- 662 [28] van der Meer JY, Poddar H, Baas BJ, Miao Y, Rahimi M, et al. (2016) Using mutability landscapes
663 of a promiscuous tautomerase to guide the engineering of enantioselective Michaelases. *Nat*
664 *Commun* 7: 10911.
- 665 [29] Risso VA, Gavira JA, Mejia-Carmona DF, Gaucher EA, Sanchez-Ruiz JM (2013) Hyperstability and
666 substrate promiscuity in laboratory resurrections of Precambrian β -lactamases. *J Am Chem Soc*
667 135: 2899-2902.
- 668 [30] Nobili A, Tao Y, Pavlidis IV, van den Bergh T, Joosten HJ, et al. (2015) Simultaneous use of in
669 silico design and a correlated mutation network as a tool to efficiently guide enzyme
670 engineering. *Chembiochem* 16: 805-810.
- 671 [31] Höppner A, Bollinger A, Kobus S, Thies S, Coscolín C, et al. (2020) Crystal structures of a novel
672 family IV esterase in free and substrate-bound form. *FEBS J* Dec 20. doi: 10.1111/febs.15680.
673 Epub ahead of print.
- 674 [32] Bauer TL, Buchholz PCF, Pleiss J (2020) The modular structure of alpha/beta-hydrolases. *FEBS J*
675 287: 1035-1053.
- 676 [33] Studer RA, Dessailly BH, Orengo CA (2013) Residue mutations and their impact on protein
677 structure and function: detecting beneficial and pathogenic changes. *Biochem J* 449: 581-594.
- 678 [34] Jack BR, Meyer AG, Echave J, Wilke CO (2016) Functional sites induce long-range evolutionary
679 constraints in enzymes. *PLoS Biol* 14: e1002452.
- 680 [35] Guzmán GI, Sandberg TE, LaCroix RA, Nyerges Á, Papp H, et al. (2019). Enzyme promiscuity
681 shapes adaptation to novel growth substrates. *Mol Syst Biol* 15: e8462.
- 682 [36] Lichtarge O, Bourne HR, Cohen FE (1996) An evolutionary trace method defines binding surfaces
683 common to protein families. *J Mol Biol* 257: 342-358.
- 684 [37] Mihalek I, Res I, Lichtarge O (2004). A family of evolution-entropy hybrid methods for ranking
685 protein residues by importance. *J Mol Biol* 336: 1265-1282.

- 686 [38] Rodriguez GJ, Yao R, Lichtarge O, Wensel TG (2010) Evolution-guided discovery and recoding of
687 allosteric pathway specificity determinants in psychoactive bioamine receptors. *Proc Natl Acad*
688 *Sci USA* 107: 7787-7792.
- 689 [39] Giunta CI, Cea-Rama I, Alonso S, Briand ML, Bargiela R, et al. (2020) Tuning the properties of
690 natural promiscuous enzymes by engineering their nano-environment. *ACS Nano* 14: 17652-
691 17664.
- 692 [40] Kabsch W (2010) XDS. *Acta Crystallogr D Biol Crystallogr* 66: 125-132.
- 693 [41] Evans PR, Murshudov GN (2013) How good are my data and what is the resolution? *Acta*
694 *Crystallogr D Biol Crystallogr* 69: 1204-1214.
- 695 [42] Winn MD, Ballard CC, Cowtan KD, Dodson EJ, Emsley P, et al. (2011) Overview of the CCP4 suite
696 and current developments. *Acta Crystallogr D Biol Crystallogr* 67: 235-242.
- 697 [43] Murshudov GN, Vagin AA, Dodson EJ (1997) Refinement of macromolecular structures by the
698 maximum-likelihood method. *Acta Crystallogr D Biol Crystallogr* 53: 240-255.
- 699 [44] Emsley P, Lohkamp B, Scott WG, Cowtan K (2010) Features and development of Coot. *Acta*
700 *Crystallogr D Biol Crystallogr* 66: 486-501.
- 701 [45] Moriarty NW, Grosse-Kunstleve RW, Adams PD (2009) Electronic Ligand Builder and
702 Optimization Workbench (eLBOW): a tool for ligand coordinate and restraint generation. *Acta*
703 *Crystallogr D Biol Crystallogr* 65: 1074-1080.
- 704 [46] Fraczekiewicz R, Braun W (1998) Exact and efficient analytical calculation of the accessible surface
705 areas and their gradients for macromolecules. *J Comput Chem* 19: 319.
- 706 [47] Guilloux VL, Schmidtke P, Tuffery P (2009) Fpocket: An open source platform for ligand pocket
707 detection. *BMC Bioinformatics* 10: 168.
- 708 [48] Katsonis P, Lichtarge O (2014) A formal perturbation equation between genotype and
709 phenotype determines the Evolutionary Action of protein-coding variations on fitness. *Genome*
710 *Res* 24: 2050-2058.
- 711 [49] Badger JH, Hoover TR, Brun YV, Weiner RM, Laub MT, et al. (2006) Comparative genomic
712 evidence for a close relationship between the dimorphic prosthecate bacteria *Hyphomonas*
713 *neptunium* and *Caulobacter crescentus*. *J Bacteriol* 188: 6841-6850.
- 714 [50] Janes LE, Kazlauskas RJ (1997) Quick E. A fast spectrophotometric method to ensure the
715 enantioselectivity of hydrolases. *J Org Chem* 62: 4560-4561.
- 716 [51] Huang J, Huo YY, Ji R, Kuang S, Ji C, Xu XW, Li J (2016) Structural insights of a hormone sensitive
717 lipase homologue Est22. *Sci Rep* 6: 28550.
- 718 [52] Ngo TD, Ryu BH, Ju H, Jang E, Park K, et al. (2013) Structural and functional analyses of a
719 bacterial homologue of hormone-sensitive lipase from a metagenomic library. *Acta Crystallogr D*
720 *Biol Crystallogr* 69: 1726-1737.
- 721 [53] Wei Y, Contreras JA, Sheffield P, Osterlund T, Derewenda U, et al. (1999). Crystal structure of
722 brefeldin A esterase, a bacterial homolog of the mammalian hormone-sensitive lipase. *Nat*
723 *Struct Biol* 6: 340-345.
- 724 [54] Dou S, Kong XD, Ma BD, Chen Q, Zhang J, et al. (2014) Crystal structures of *Pseudomonas putida*
725 esterase reveal the functional role of residues 187 and 287 in substrate binding and chiral
726 recognition. *Biochem Biophys Res Commun* 446: 1145-1150.
- 727 [55] Lua RC, Lichtarge O (2010) PyETV: A PyMOL evolutionary trace viewer to analyze functional site
728 predictions in protein complexes. *Bioinformatics* 26: 2981-2982.
- 729 [56] Altschul SF, Gish W, Miller W, Myers EW, Lipman DJ (1990) Basic local alignment search tool. *J*
730 *Mol Biol* 215: 403-410.
- 731 [57] UniProt Consortium (2019) UniProt: a worldwide hub of protein knowledge. *Nucleic Acids Res*
732 47: D506-D515.
- 733 [58] Klemetsen T, Raknes IA, Fu J, Agafonov A, Balasundaram SV, et al. (2018) The MAR databases:
734 development and implementation of databases specific for marine metagenomics. *Nucleic Acids*
735 *Res* 46: D692-D699.

736 [59] Jurcik A, Bednar D, Byska J, Marques SM, Furmanova K, et al. (2018) CAVER Analyst 2.0: analysis
737 and visualization of channels and tunnels in protein structures and molecular dynamics
738 trajectories. *Bioinformatics* 34: 3586-3588.